PHYLOGENETICS

10.1126/sciadv.1500162

Adaptive evolutionary paths from UV reception to sensing violet light by epistatic interactions

Shozo Yokoyama,[1]* Ahmet Altun,[2] Huiyong Jia,[1] Hui Yang,[1] Takashi Koyama,[1] Davide Faggionato,[1] Yang Liu,[1] William T. Starmer[3]

Ultraviolet (UV) reception is useful for such basic behaviors as mate choice, foraging, predator avoidance, communication, and navigation, whereas violet reception improves visual resolution and subtle contrast detection. UV and violet reception are mediated by the short wavelength–sensitive (SWS1) pigments that absorb light maximally (λ_{max}) at ~360 nm and ~395 to 440 nm, respectively. Because of strong nonadditive (epistatic) interactions among amino acid changes in the pigments, the adaptive evolutionary mechanisms of these phenotypes are not well understood. Evolution of the violet pigment of the African clawed frog (*Xenopus laevis*, λ_{max} = 423 nm) from the UV pigment in the amphibian ancestor (λ_{max} = 359 nm) can be fully explained by eight mutations in transmembrane (TM) I–III segments. We show that epistatic interactions involving the remaining TM IV–VII segments provided evolutionary potential for the frog pigment to gradually achieve its violet-light reception by tuning its color sensitivity in small steps. Mutants in these segments also impair pigments that would cause drastic spectral shifts and thus eliminate them from viable evolutionary pathways. The overall effects of epistatic interactions involving TM IV–VII segments have disappeared at the last evolutionary step and thus are not detectable by studying present-day pigments. Therefore, characterizing the genotype-phenotype relationship during each evolutionary step is the key to uncover the true nature of epistasis.

INTRODUCTION

In 1918, Ronald Aylmer Fisher introduced the notion of "dual epistacy" to explain the deviations from linearity due to interactions between different genes involved in producing quantitative characters. He concluded that because of their second-order contribution, nonadditive (epistatic) interactions only provided small changes in phenotypes, and thus, epistasis could be ignored (*1*). On the other hand, Sewall Wright argued that epistatic effects were common and that most complex characters are expected to have netlike relationships among genes, and thus, epistasis is of central importance to the evolutionary process (*2*). This difference in viewpoint remains a primary question in evolutionary biology (*3*).

In laboratories, epistatic interactions in microorganism systems can be controlled and analyzed using short- and long-term experimental evolution (*4*–*9*). In contrast, using vertebrate systems, it is extremely difficult to perform such experimental evolution of phenotypic adaptation. However, light-sensitive visual pigments provide a useful model system to investigate the adaptive evolutionary steps and their functional changes that have occurred over long time periods (*10*–*13*). One possible evolutionary trajectory might reveal a stepwise series of single amino acid replacements that additively accumulate changes in the capacity to detect specific wavelengths of light (*14*, *15*); alternatively, the stepwise changes could involve one or more interactions with previous changes that produce epistatic effects (*16*).

By the early 1930s, it was already known that the behavior of many insects was strongly affected by their ability to detect and see ultraviolet (UV) light (*17*). It took about 60 additional years, but it became clear that a wide range of vertebrates also use UV reception for such basic behaviors as mate choice, foraging, predator avoidance, communication, and navigation (*18*–*21*); however, human and many other species have replaced the ancestral UV reception by violet (or blue) reception even when they receive abundant UV light in their environment (*22*). Newly evolved eye structures of the latter animals prevent their retinas from receiving UV light, protecting them from UV damage, whereas the more recently evolved violet reception have improved their visual resolution and subtle contrast detection (*23*). In the avian ancestor, UV reception was lost, but more recently, certain present-day species have switched back to UV reception, which, in turn, became critical in orienting themselves using the sun compass during migration (*19*, *24*).

UV and violet reception are regulated by the short wavelength–sensitive (SWS1) pigments that absorb light maximally (λ_{max}) at ~360 nm and 390 to 440 nm, respectively (*22*). Because of strong nonadditive (epistatic) interactions among adaptive mutations within each SWS1 pigment (*10*, *11*), the potential of new mutations for changes in color vision can be significantly modified or constrained during evolution by existing and subsequent mutations (*16*, *25*–*29*). It is widely accepted that the variable λ_{max}s of SWS1 pigments are generated by mutations in the transmembrane helices (TM) I–III of SWS1 pigments (*30*–*34*), which can be divided into six segments, roughly containing TM I, II, III, IV, V, and VI–VII (Fig. 1 and fig. S1). Indeed, the evolution of the violet-sensitive pigment in the African clawed frog (frog-423, λ_{max} = 423 nm) from its UV-sensitive ancestral amphibian pigment (AncAmphibian-359, λ_{max} = 359 nm) can be fully explained by eight mutations in TM I–III, each with only small or no individual effect, but TM IV–VII were also suspected to have been involved during frog-423 evolution (*34*). Therefore, frog-423 offers a rare opportunity to test the commonly held view that only TM I–III are involved in the spectral tuning of SWS1 pigments and also to learn the true nature of epistatic interactions in evolution.

To interpret the subsequent sections, the following explanation of nomenclature with examples may be helpful (Table 1). (i) When

[1]Department of Biology, Emory University, Atlanta, GA 30322, USA. [2]Department of Physics and Department of Genetics and Bioengineering, Fatih University, Istanbul 34500, Turkey. [3]Department of Biology, Syracuse University, Syracuse, NY 13244, USA.
*Corresponding author. E-mail: syokoya@emory.edu

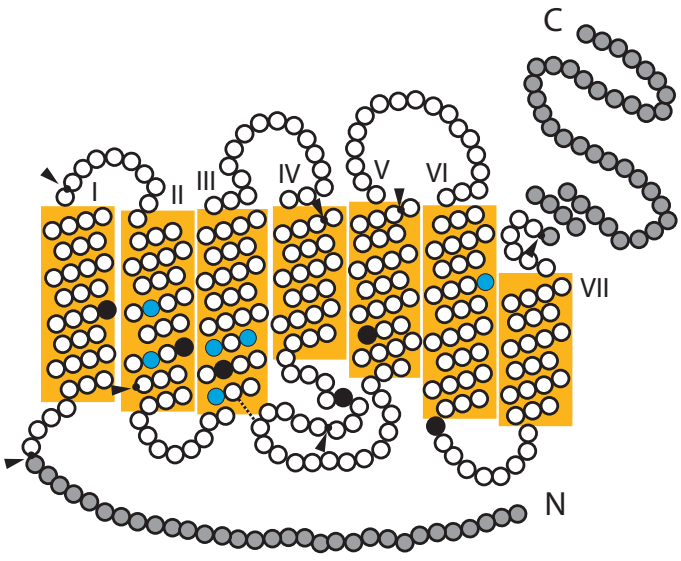

Fig. 1. Two-dimensional model of AncAmphibian-359. Twelve amino acid changes that shifted the λ_{max} are shown in black (highly critical) and blue (less so). Seven arrowheads indicate restriction recognition sites (fig. S1). The model is after Palczewski (*46*).

referring to chimeric pigments, A2F, for example, means that the TM II of AncAmphibian-359 was replaced by the corresponding segment of frog-423, whereas A24F means that TM II and IV were replaced. (ii) E113 refers to glutamic acid at site 113. When referencing amino acid replacements, E113D, for example, means that glutamic acid (E) is replaced by aspartic acid (D) at position 113 in AncAmphibian-359; D113E can also be introduced into frog-423. (iii) $F_{1.0}86I_{0.52}$ indicates that phenylalanine (F) is replaced by isoleucine (I) at site 86, where F and I have posterior probabilities (PPs) of 1.0 and 0.52, respectively. (iv) ζ_{86} is the magnitude of the λ_{max} shift (or $\Delta\lambda_{max}$) caused by an amino acid change at position 86 (for example, F86M) (iv) ζ_{86}. When F86M and T93P are introduced into AncAmphibian-359, the $\Delta\lambda_{max}$ caused by these mutations is given by $\zeta_{86} + \zeta_{93} + \zeta_{86\times93}$, where $\zeta_{86\times93}$ is the epistatic effect caused by F86M and T93P. (v) θ_2 is the $\Delta\lambda_{max}$ caused by replacing TM II of AncAmphibian-359 by the corresponding segment of frog-423, and θ_{23} is the epistatic effect caused by TM II–III of frog-423.

Table 1. Abbreviations and explanation of key terms with examples.

SWS1 pigment	The short wavelength–sensitive type 1 visual pigment
λ_{max}	The wavelength of maximal absorption
$\Delta\lambda_{max}$	The magnitude of λ_{max} shift
TM	Transmembrane helix of a visual pigment
PP	Posterior probability of an amino acid inferred
SBN	Schiff base nitrogen—when it is unprotonated, a pigment is UV-sensitive; otherwise, it is violet-sensitive
A2F	The chimeric pigment, in which the TM II of AncAmphibian-359 was replaced by the corresponding segment of frog-423
A24F	The chimeric pigment, in which the TM II and IV of AncAmphibian-359 were replaced by the corresponding segments of frog-423
E113	Amino acid glutamic acid (E) at site 113
E113D	Amino acid change from glutamic acid (E) to aspartic acid (D) at site 113
$F_{1.0}86I_{0.52}$	Phenylalanine (F) is replaced by isoleucine (I) at site 86, where F and I have PPs of 1.0 and 0.52, respectively.
ζ_{86}	The $\Delta\lambda_{max}$ of AncAmphibian-359 caused by an amino acid change, F86M
$\zeta_{86\times93}$	The $\Delta\lambda_{max}$ of AncAmphibian-359 caused by the epistatic interaction between F86M and T93P
θ_2	The λ_{max} shift of AncAmphibian-359 caused by replacing its TM II by the corresponding segment of frog-423
θ_{23}	The λ_{max} shift of AncAmphibian-359 caused by the epistatic interaction between the TM II and III of frog-423

RESULTS

New adaptive mutations

To find the amino acid changes in TM IV–VII that have contributed to the λ_{max} shift during frog-423 evolution, we have constructed various chimeric pigments between AncAmphibian-359 and frog-423 and introduced mutations into them. The results show that A2F has a λ_{max} of 383 nm and series of chimeric pigments A24F, A25F, A26F, and A2456F increase the λ_{max} of A2F by 8, 3, 7, and 21 nm, respectively; hence, TM IV–VII are also involved in the spectral tuning in frog-423 (Fig. 2). When we introduce I179M (in TM IV), L207I (TM V), and V256F and N277T (or V256F/N277T) (both in TM VI) into A2F, the mutant pigments achieve new λ_{max}s of 394, 386, and 387 nm, respectively, and the four mutations in A2F together increase the λ_{max} to 403 nm, which is virtually identical to the λ_{max} of A2456F (Fig. 2). Hence, the actual number of adaptive mutations that contributed to the frog-423 evolution is 12, which is distributed throughout TM I–VI (Fig. 1, black and blue circles). As described below, the six amino acid sites in black play critical roles in causing λ_{max} shift and are distinguished from the other sites in blue. Consequently, the commonly used tenet on the spectral tuning in SWS1 pigments is rejected.

Ancestral amino acids

We inferred the 12 amino acids present at the nodes of a phylogenetic tree during the frog-423 evolution by using 14 representative pigments (fig. S2) and the maximum likelihood–based Bayesian method [phylogenetic analysis by maximum likelihood (PAML) (*35*) with Jones-Taylor-Thornton (JTT) and Whelan and Goldman (WAG) substitution models]. In particular, we inferred the amino acids at the 12 sites of three ancestral pigments in a composite tree of 14 representative SWS1 pigments: (i) AncAmphibian-359; (ii) the common ancestor of African clawed frog, Western clawed frog, and bullfrog pigments (AncFrog); and (iii) the common ancestor of the two clawed frog pigments (AncClawed-frog) (fig. S2). The 12 amino acids predicted using the two models have very similar PPs and are highly consistent (table S1). With the exception of site 109, the amino acids of AncAmphibian-359 have a PP of >0.95 and are highly reliable. For AncClawed-frog, all 12 amino acids have a PP of >0.90. For AncFrog, the amino acids (sites 113 to 277) in TM III–VI are

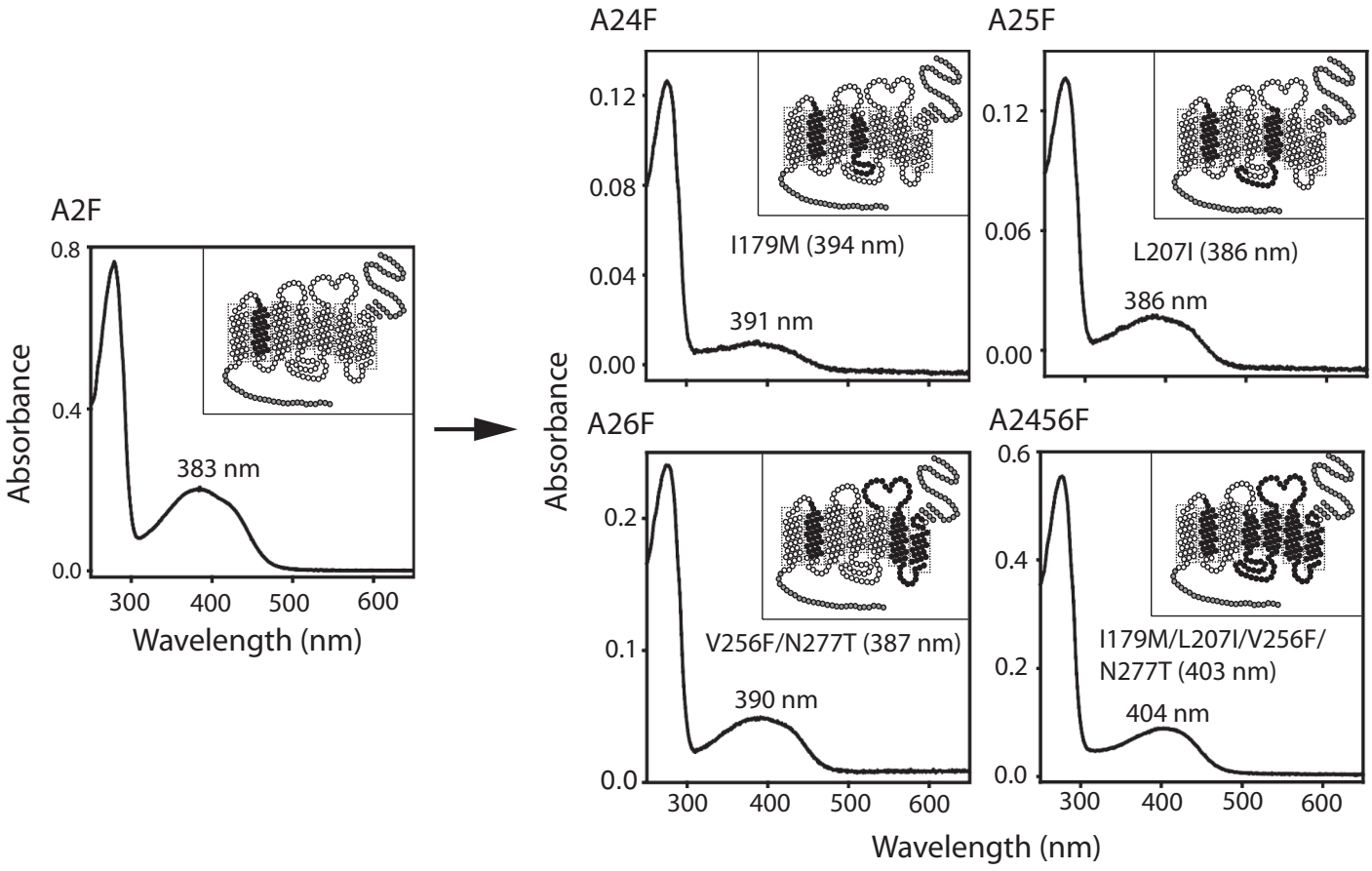

Fig. 2. The absorption spectra of various chimeric pigments that are derived from A2F. The white and black segments of the visual pigment (inset) indicate those of AncAmphibian-359 and frog-423, respectively. The λ_{max}s of A2F mutants with various amino acid changes are also shown in parentheses.

more reliable than those (sites 49 to 93) in TM I-II. When the frog-423 evolution is divided into three stages, that is, from AncAmphibian-359 to AncFrog (stage 1), from AncFrog to AncClawed-frog (stage 2), and from AncClawed-frog to frog-423 (stage 3), most of the adaptive changes occurred in stages 1 and 2 (Fig. 3), in which the levels of reliabilities of the 12 inferred amino acids using the JTT model are also indicated using the logos.

At amino acid site 86, the JTT model of AncAmphibian-359 predicts phenylalanine (F) with a PP of 1.0, whereas that of AncFrog can be I86 or M86 or F86 with PPs of 0.52, 0.41, and 0.05, respectively (table S1). Therefore, at this position, the most probable occurrence of $F_{1.0}86I_{0.52}$ was during stage 1 of the frog-423 evolution, whereas the frog-423 evolution was completed by $I_{0.52}86M_{1.0}$ at stage 2. Alternatively, $F_{1.0}86M_{0.41}$ could have occurred during stage 1 of the frog-423 evolution. Extending the same argument to other sites (table S1), it is likely that $V_{0.96}91I_{0.81}$ and $T_{0.53}93P_{1.0}$ occurred at stages 1 and 2, respectively. Hence, considering the entire TM II segment, V91I, and possibly F86M, preceded T93P. Similarly, the most probable amino acid replacements in TM III are $V_{0.45}109A_{0.99}$ (stage 2) (or $V_{0.61}109A_{0.25}$ in stage 1), $E_{0.94}113D_{0.98}$ (stage 2), $L_{0.99}116V_{0.94}$ (stage 1), and $S_{0.99}118T_{0.99}$ (stage 1); therefore, L116V and S118T, and possibly V109A, preceded E113D. The most probable occurrence of $I_{0.99}179M_{0.99}$ was during stage 3 in TM IV and $L_{1.0}207I_{0.99}$ at stage 1 in TM V. In TM VI–VII, $N_{0.98}277T_{0.99}$ (stage 1) occurred much earlier than $V_{1.0}256T_{1.0}$ (stage 3). A more specific order of the six critical mutation accumulations can be predicted by considering their roles in gradual phenotypic adaptation by recapitulating evolutionary trajectories (see below).

Amino acid replacements and TM changes

Given 12 critical amino acid replacements, the total number of possible evolutionary trajectories is 12! (or ~500 million). Because of this prohibitive number, we investigated the possibility of using the TM segments to capture the effects of the amino acid replacements within them. When a TM change is dominated by one amino acid replacement, we consider that a chimeric pigment with the TM change effectively represents the amino acid replacements. Within TM II, F86M and T93P together increase the λ_{max} of AncAmphibian-359 ($\zeta_{86} + \zeta_{93} + \zeta_{86\times93}$) by 35 nm, but when V91I precedes one of these mutations, the λ_{max} only increases by 21 nm (Table 2), where ζ_i is the λ_{max} shift caused by an amino acid change *i* (Table 1). Hence, V91I determines the effect of the TM II replacement on the upper limit of λ_{max} shift. Within TM III, V109A, L116V, and S118T do not shift the λ_{max} of AncAmphibian-359 at all ($\zeta_{109} + \zeta_{116} + \zeta_{118} + \zeta_{109\times116} + \zeta_{109\times118} + \zeta_{116\times118} + \zeta_{109\times116\times118} = 1$ nm), whereas E113D in AncAmphibian-359 decreases the λ_{max} by 4 nm. However, when V109A, L116V, and S118T are followed by E113D, the significant effects of epistatic interactions occur between V109A and E113D (λ_{max} shift, or $\Delta\lambda_{max} = 14$ nm), and among V109A, E113D, and L116V ($\Delta\lambda_{max} = 21$ nm); V109A, E113D,

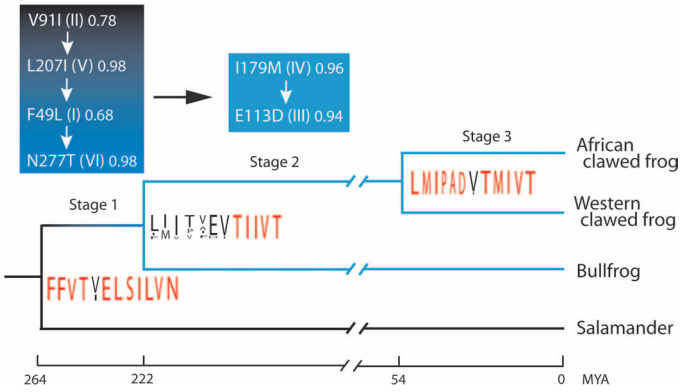

Fig. 3. The most probable pattern of the amino acid replacements during amphibian pigment evolution. The evolutionary tree of frog-423 and orthologous amphibian pigments, where the divergence times at the three nodes were obtained from the TimeTree of Life web server (www.timetree.org). Six functionally critical amino acid replacements are shown above, where the numbers are the products of the PPs of the two amino acids inferred and indicate the likelihoods that these changes occur at a specific evolutionary stage. The PPs are taken from the maximum likelihood–based Bayesian method (*35*) with the JTT model, and the logos of amino acids at 12 critical sites for the three ancestral amphibian pigments indicate their support values, where amino acids in red have PPs >0.95 (table S1). Branches and boxes in black and blue indicate UV and violet sensitivities, respectively. Sharing only T118, I207, and T277 among the 12 critical amino acids of frog-423, the bullfrog SWS1 pigment must have achieved its violet sensitivity (*55*) using an entirely different mechanism. (For the sequence of mutation accumulations, see the "Evolutionary trajectories" section. MYA, million years ago.)

and S118T ($\Delta\lambda_{max}$ = 20 nm), and V109A, E113D, L116V and S118T ($\Delta\lambda_{max}$ = −6 nm). The four mutations together increase the λ_{max} by 49 nm (Table 2). As described in the next section, the TM III change occurred toward the end of the frog-423 evolution; in that case, the λ_{max} shift caused by the TM III change is only 15 nm. This value is very close to the λ_{max} shift caused by E113D near the end of the frog-423 evolution, which can be seen from the reverse experiment of D113E in frog-423 ($\Delta\lambda_{max}$ = −12 nm) (*36*). Therefore, the significant epistatic interactions among V109A, L116V, and S118T in TM III and the amino acid changes in the other TMs did not occur during the frog-423 evolution. These observations suggest that F49L, V91I, E113D, I179M, L207I, and N277T roughly correspond to TM I, II, III, IV, V, and VI–VII replacements, respectively (Fig. 1, black circles).

To establish the one-to-one relationship between TM replacement and λ_{max} shift, we constructed all 63 possible (6 single and 57 multiple) chimeric pigments, performed in vitro assays (*37*), and attempted to evaluate their λ_{max} values. We then found that nine (A34F, A35F, A36F, A134F, A345F, A346F, A356F, A1345F, and A1346F) pigments were nonfunctional. The other chimeric pigments have λ_{max}s between 359 and 423 nm (table S2, nonfunctional pigments in bold italics). Because of its involvement in all nine nonfunctional pigments, the TM III change seems to be causing the nonfunctionalization. However, much to our surprise, the real cause is traced to the TM IV–VII changes.

Chemical impairments

The function of visual pigments is to convert light waves into an electrical signal. This phototransduction process depends on how the amino acid sequence interacts with 11-*cis*-retinal and is sensitive to the size and shape of the retinal binding pocket. In UV-sensitive pigments, Schiff base nitrogen (SBN) covalently bound to 11-*cis*-retinal is unprotonated, whereas its neighboring E113 is protonated (*38*). In AncAmphibian-359, its SBN and E113 are connected by an H-bond, making the pigment structurally stable and functional (fig. S3). In A3F, D113 forms an H-bond with S90 rather than SBN; the space between D113 and SBN is filled with a water molecule that is stabilized by two H-bonds with SBN and D113 (Fig. 4A). A34F becomes nonfunctional because the M179 side chain cleaves the C110-C187 disulfide bond and places D113 near the protein surface (Fig. 4B). A35F and A36F become nonfunctional because they cannot achieve the distances larger than 2.20 Å between 11-*cis*-retinal and Y265 (A35F, Fig. 4C) or W191 (A36F, Fig. 4D). The common feature of the nine nonfunctional pigments is that the TM IV–VII changes either preceded or followed A3F or A13F that cause the two largest single-step λ_{max} shifts of 51 to 58 nm (table S2). The evolutionary significance of chemical impairments can also be illustrated by comparing A13F and A23F, which shift the λ_{max} by 58 and 62 nm, respectively, and are very similar. However, the two-step λ_{max} shifts of A13F are 0 nm followed by 58 nm, but the corresponding values for A23F are 24 and 38 nm and are more evenly distributed. Hence, the TM IV–VII changes effectively terminate the drastic phenotypic change by either making the retinal binding pocket too small or by causing other detrimental structural changes.

Evolutionary trajectories

The pattern of mutation accumulation, epistatic interactions among mutations, and premature termination of evolutionary trajectories with drastic λ_{max} shifts all point to one thing: frog-423 gradually achieved its λ_{max}. To recapitulate the processes of frog-423 evolution, we constructed all 6! (or 720) possible evolutionary trajectories from AncAmphibian-359 to frog-423. The results show that 244 trajectories are prematurely terminated because of the nine nonfunctional pigments (fig. S4A) and the A1F, A2F, A3F, A4F, A5F, or A6F pigments generate 92, 120, 38, 70, 78, and 78 evolutionarily acceptable trajectories, respectively (fig. S4B). To extract biological significance of these data, it is useful to consider the orthologous pigment in humans (human-414, λ_{max} = 414 nm), which also attained its violet sensitivity by multiple adaptive mutations (F46T, F49L, T52F, F86L, T93P, A114G, and S118T) in TM I–III (*16*). Human-414 gradually achieved its current λ_{max} ($\Delta\lambda_{max}$ < 25 nm) at every evolutionary step almost exclusively by epistatic interactions among the seven mutations.

By recapitulating the evolutionarily acceptable trajectories from AncAmphibian-359 to frog-423, we can see that the magnitudes of λ_{max} shifts caused by specific TM replacements significantly vary depending on which TM replacement(s) they follow (table S3). For example, the most prominent individual effects on the λ_{max} shift come from TM II change ($\Delta\lambda_{max}$ = 24 nm) and III change ($\Delta\lambda_{max}$ = 51 nm). However, if the TM II change occurs in A456F, then the $\Delta\lambda_{max}$ increases to 44 nm. On the other hand, as we saw earlier, if the TM III change occurs at the last evolutionary step, the $\Delta\lambda_{max}$ is only 15 nm. Moreover, TM I, IV, V, and VI changes cause no λ_{max} shift individually, but when TM I change occurs in A245F, it causes a $|\Delta\lambda_{max}|$ of 11 nm, whereas when TM IV, V, and VI changes occur in A1356F, A136F, and A135F, respectively, they cause a $|\Delta\lambda_{max}|$ of 16 to 22 nm.

These evolutionary trajectories can be classified into two groups depending on whether or not the evolutionary paths that contain at least one $\Delta\lambda_{max}$ burst during evolution. All evolutionary trajectories

Table 2. The effects of amino acid replacements on the λ_{max} shift in AncAmphibian-359.*

TM II			TM III				λ_{max} (nm)	λ_{max} shift	
F86M	V91I	T93P	V109A	E113D	L116V	S118T		$\Delta\lambda_{max}$ (nm)	Wavelength ± SE (nm)
0	0	0	0	0	0	0	359		
1	0	0	0	0	0	0	361	ζ_{86}	2 ± 1.41
0	1	0	0	0	0	0	362†	ζ_{91}	3 ± 1.41
0	0	1	0	0	0	0	359	ζ_{93}	0 ± 1.41
1	0	1	0	0	0	0	394	$\zeta_{86\times93}$	33 ± 2.0
1	1	1	0	0	0	0	380	$\zeta_{86\times91\times93}$	−17 ± 2.8
0	0	0	1	0	0	0	360	ζ_{109}	1 ± 1.41
0	0	0	0	1	0	0	355	ζ_{113}	−4 ± 1.41
0	0	0	0	0	1	0	359	ζ_{116}	0 ± 1.41
0	0	0	0	0	0	1	361	ζ_{118}	2 ± 1.41
0	0	0	1	1	0	0	370	$\zeta_{109\times113}$	14 ± 2.0
0	0	0	1	0	1	0	359	$\zeta_{109\times116}$	−1 ± 2.0
0	0	0	1	0	0	1	361	$\zeta_{109\times118}$	−1 ± 2.0
0	0	0	0	1	1	0	356†	$\zeta_{113\times116}$	1 ± 2.0
0	0	0	0	1	0	1	357	$\zeta_{113\times118}$	0 ± 2.0
0	0	0	0	0	1	1	360	$\zeta_{116\times118}$	−1 ± 2.0
0	0	0	1	1	1	0	391	$\zeta_{109\times113\times116}$	21 ± 2.8
0	0	0	1	1	0	1	391	$\zeta_{109\times113\times118}$	20 ± 2.8
0	0	0	1	0	1	1	360	$\zeta_{109\times116\times118}$	1 ± 2.8
0	0	0	0	1	1	1	359†	$\zeta_{113\times116\times118}$	2 ± 2.8
0	0	0	1	1	1	1	408	$\zeta_{109\times113\times116\times118}$	−6 ± 2.8

*Numbers 0 and 1 indicate the amino acid of AncAmphibian S1 and that of frog S1, respectively. †These data are newly obtained; others are taken from (*34*).

started with A1F, A3F, A4F, A5F, and A6F have a burst of the $\Delta\lambda_{max}$ >25 nm (shown in red paths, fig. S4B), whereas 54 of 120 evolutionarily acceptable trajectories started with A2F are characterized by $\Delta\lambda_{max}$ <25 nm nm at every evolutionary step (black paths, fig. S4B). Moreover, 25 of these 54 trajectories are characterized by the more restricted condition of $\Delta\lambda_{max}$ <20 nm at every mutational step after TM II replacement and are closely clustered along the diagonal paths (black paths, Fig. 5).

These 25 trajectories are best represented by A251643F that is consistent with the results based on PAML using the JTT and WAG models. That is, the amino acid changes in the ancestral pigments suggest that TM I, II, V, and VI changes and TM III and IV changes occurred in stages 1 and 2 of frog-423 evolution, respectively (Fig. 3). At stage 1, the TM II change has the smallest λ_{max} shift; after that, the two evolutionary sequences could have increased the λ_{max} equally smoothly: 1) TM V change ($\Delta\lambda_{max}$ = 3 nm) followed by TM I change ($\Delta\lambda_{max}$ = 6 nm) and TM VI change ($\Delta\lambda_{max}$ = 5 nm), in that order, or 2 TM I change ($\Delta\lambda_{max}$ = 6 nm) followed by TM V change ($\Delta\lambda_{max}$ = 3 nm) and TM VI change ($\Delta\lambda_{max}$ = 5 nm), in that order (table S3). Because the TM V change will stop the early establishment of the TM III change with a burst of λ_{max} shift, A2516F is the most likely sequence among the 25 trajectories. At stage 2, the evolutionary sequence of the TM IV change ($\Delta\lambda_{max}$ = 11 nm) followed by the TM III change ($\Delta\lambda_{max}$ = 15 nm) is more gradual than that of the TM III change ($\Delta\lambda_{max}$ = 24 nm) followed by the TM IV change ($\Delta\lambda_{max}$ = 2 nm) (table S3). Hence, A251643F has one of the smoothest λ_{max} shifts (Fig. 5, black path with open circles; table S3, bold italics). In turn, this implies that the amino acid replacements V91I, L207I, F49L, N277T, I179M, and E113D occurred in that order (Fig. 3).

Epistatic interactions

To determine the individual effects and the effects of all combinations of 12 amino acid replacements on the λ_{max} shift, we traced A251643F as a representative trajectory of frog-423 evolution. Solving linear equations of the λ_{max}s of the 63 chimeric pigments, in which the highest level of λ_{max} shifts caused by the nonfunctional pigments is zero (*16*), we evaluated six individual $\Delta\lambda_{max}$s (θ_i, i = 1, 2, …, 6) and 57 other θs with multiple interactions. These θs and the corresponding pure epistatic interactions among TM I–VII (θ_0) without any individual amino acid effects are very similar (table S2). The λ_{max} shifts can be explained by the individual and pure epistatic interactions among TM I–VII

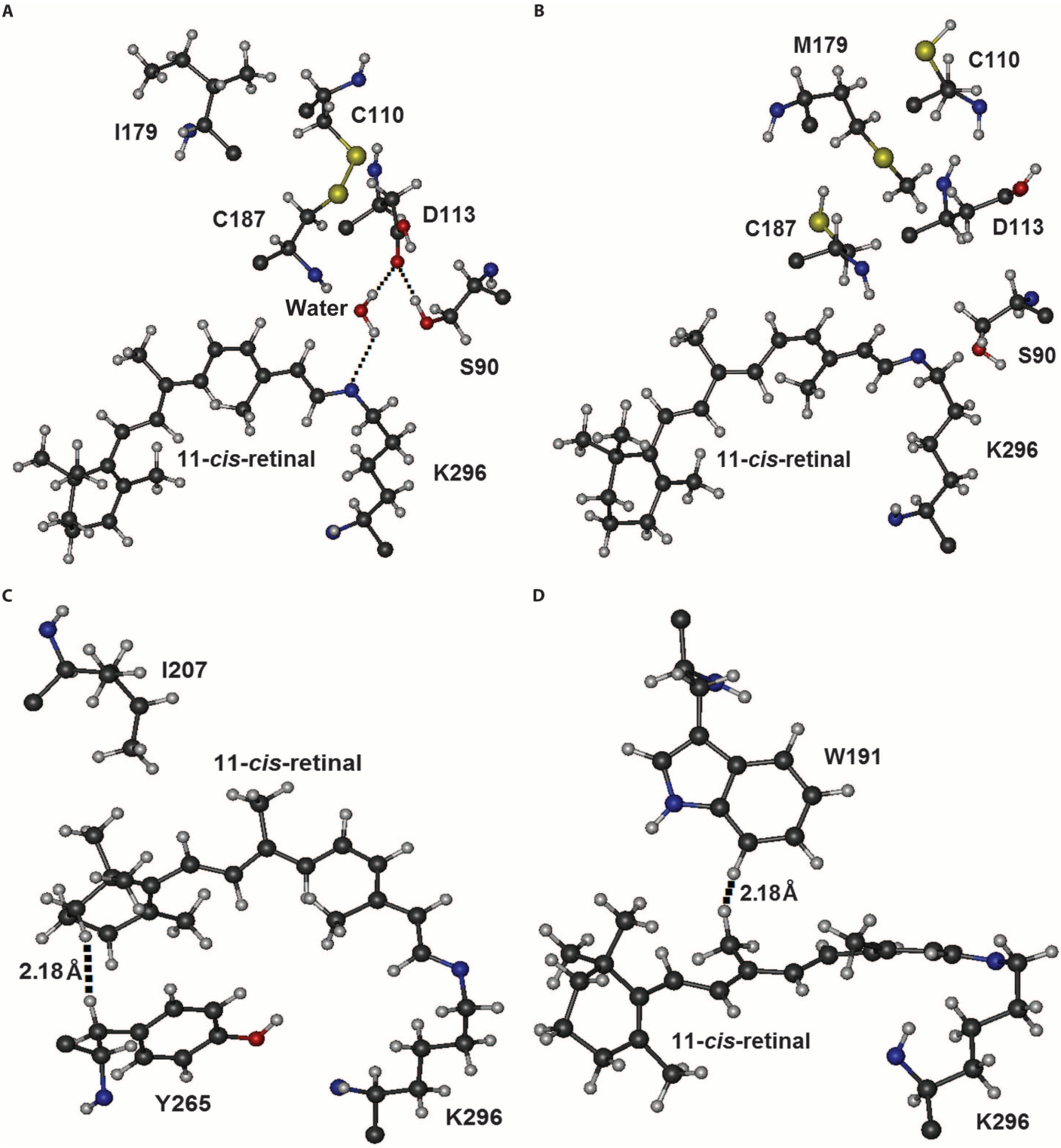

Fig. 4. The tertiary structures of SWS1 pigments. (**A**) A3F. (**B**) A34F. (**C**) A35F. (**D**) A36F. Black, blue, red, and white molecules represent carbon, nitrogen, oxygen, and hydrogen atoms, respectively.

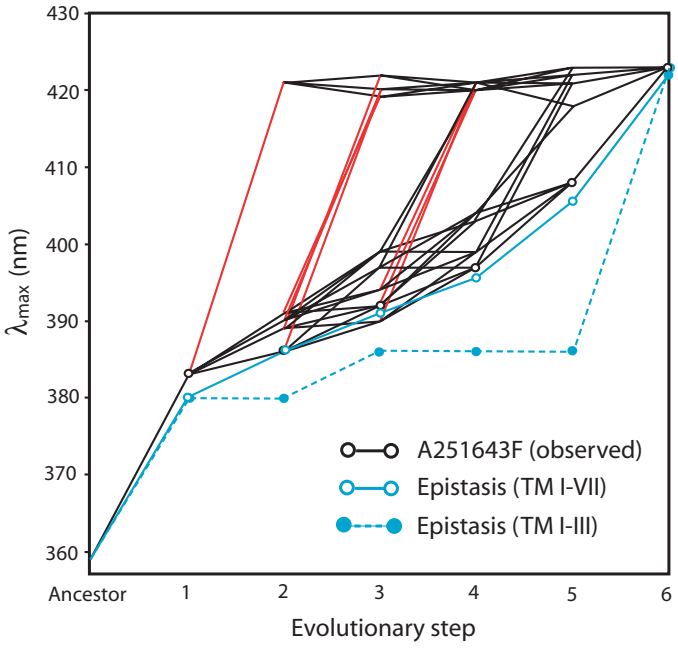

Fig. 5. All 120 possible evolutionarily accessible trajectories of A2F. Two levels of $\Delta\lambda_{max}$ (<25 or > 25 nm) are shown by black and red lines, respectively. A251643F (in black) is compared to those with pure epistatic interactions among TM I–VII (in blue) and TM I–III (in blue broken line).

changes (Fig. 5, blue path with open circles). Each evolutionary step of A251643F can also be explained by θs without using the λ_{max}s of the nine nonfunctional pigments; in that case, many epistatic interaction terms cannot be individually assessed (table S4). When all individual and epistatic interactions are considered, the largest individual effects θ_2 and θ_3 are followed by θ_{1235}, θ_{1236}, θ_{12356}, and θ_{13456} with a sum of 132 nm, which are countered by θ_{23}, θ_{123}, θ_{135}, θ_{234}, θ_{1235}, θ_{1236}, θ_{1356}, θ_{123456}, and others (table S2). Hence, TM III change has a significant impact on frog-423 evolution through its individual effect as well as epistatic interactions with the other TM changes. A fascinating thing about these epistatic interactions is that the sum of all 56 θs (or θ_0s) that involve TM IV–VII changes of frog-423 is only +1, showing that the overall effects of epistatic interactions of TM IV–VII changes have disappeared at the last evolutionary step (table S2) (*34*).

The true nature of epistatic interactions involving TM IV–VII emerges when we completely exclude their effects in recapitulating A251643F. That is, the λ_{max}s of A2F, A25F, A251F, A2516F, and A25164F are underestimated by 0, 6, 6, 11, and 22 nm, respectively, which, in turn, requires the trajectory A251643F to achieve a prohibitively high λ_{max} shift of 37 nm (Fig. 5, blue broken line with blue circles). Therefore, TM IV–VII provided a molecular environment during the frog-423 evolution that allowed access to a gradual evolutionary pathway.

DISCUSSION

To date, all mutations that have caused the variable λ_{max}s of SWS1 pigments have been localized in the TM I–III (*30*–*34*). However, we have seen that the violet sensitivity of frog-423 evolved by 12 mutations that are distributed in TM I–VI. The evolution of frog-423 is characterized by the gradual λ_{max} shift caused by strong epistatic interactions among these mutations. In particular, the epistatic interactions of the amino acids in TM IV–VII with the other adaptive mutations in TM I–III prematurely terminated evolutionary trajectories whenever ancestral pigments could have caused extreme shifts in λ_{max}. In human-414, T52F in TM I played a similar function; if T52F occurred first or in the early evolutionary stages of human-414, then these mutants became structurally unstable (*16*). The latter cases effectively required a future evolutionary step to incorporate a prohibitive burst of $\Delta\lambda_{max}$ >25 nm.

The origin of visual pigments may go back to well before 800 million years ago (*39*), and the vertebrate ancestor already had five different types of visual pigments (*12*, *40*, *41*). During this long history, most vertebrates have retained E113 in their visual pigments. The clawed frogs are unique among them, having incorporated E113D into their SWS1 pigments (Fig. 3). E113 is structurally critical, serving as the SBN counterion and regulating the λ_{max}s of visual pigments (*42*–*46*). However, in laboratories, visual pigments with mutations such as E113D, E113N, E113Q, and E113A were found to be functional (*45*), suggesting that various mutations occurred at position 113 of visual pigments in the past. The evolutionary novelty of the clawed frog SWS1 pigments probably took place because E113D occurred at the right time and in the right molecular environment. Our results suggest that this mutation occurred toward the end of frog-423 evolution. This timing and the specific epistatic interactions with other mutations V109A, L116V, and S118T were the key factors in determining the specific magnitude of λ_{max} shift needed for the clawed frogs to adapt to their specific ecological environment.

Current mutagenesis results suggest that violet pigments of scabbardfish (*Lepidopus fitchi*), bovine (*Bos taurus*), wallaby (*Macropus eugenii*), and elephant (*Loxodonta africana*) largely evolved by the deletion of F86 (*47*), F86Y (*32*), F86Y (*11*), and F86S (*48*), respectively, and that the reversion of a recent ancestral avian pigment largely occurred by S90C (*49*, *50*). These mutations seem to have caused λ_{max} shifts of 35 to 70 nm in one evolutionary step. However, the $|\Delta\lambda_{max}|$ values caused by S90C in various pigments vary between 0 and 45 nm (*10*, *11*). Moreover, the F86 deletion in the SWS1 pigment of the vertebrate ancestor only increases the λ_{max} by 19 nm, which is still 43 nm smaller than the λ_{max} of the scabbardfish pigment. These observations imply that additional critical mutations are involved and epistatic interactions are operating in most of the SWS1 pigments as well. Knowing that identical mutations can have markedly different effects on the λ_{max} shift during evolution (for example, TM II and TM III changes, table S3), in future studies, it would not be surprising to find that seemingly large changes in λ_{max} in a single evolutionary step are actually the accumulation of gradual changes.

As noted in the beginning, it is difficult to perform experimental evolution of phenotypic adaptation for vertebrates. However, as exemplified by our evolutionary analyses of frog-423, we can obtain similar information by (i) engineering and manipulating the phenotypes of ancestral molecules (*14*, *22*, *29*, *51*), (ii) examining the adaptive significance by comparing the phenotypic changes to their new molecular and ecological environments (*22*, *29*), (iii) determining the order of adaptive mutations by locating them in various branches in a phylogenetic tree (*40*, *52*, *53*), and (iv) experimentally recapitulating all possible evolutionary trajectories (*16*). Chemical structural analyses added a new dimension to our understanding of hidden epistatic interactions, which show that structurally stable protein structures lay the foundation for

the evolutionary potential of adaptive mutations. Manipulating ancestral molecules alleviates the potentially confusing mutagenesis results caused by analyzing present-day molecules with variable molecular environments (*10*, *11*). Establishing the one-to-one relationship between an SWS1 pigment and UV/violet reception by manipulating ancestral molecules and their phenotypes is a significant development in that direction.

MATERIALS AND METHODS

Phylogenetic analyses

To study the order of amino acid replacements in the frog-423 lineage, we considered the composite tree of SWS1 pigments sampled from 14 species: the lamprey (*Geotria australis*, GenBank accession no. AY366495), medaka (*Oryzias latipes*, AB223058), African clawed frog (*Xenopus laevis*, U23463), Western clawed frog (*Xenopus tropicalis*, NM_001126076), bullfrog (*Rana catesbeiana*, AB001983), salamander (*Ambystoma tigrinum*, AF038948), chameleon (*Anolis carolinensis*, AF134192), gecko (*Gekko gecko*, AY024356), sunbeam (*Xenopeltis unicolor*, FJ497234), chicken (*Gallus gallus*, M92039), zebra finch (*Taeniopygia guttata*, AF222331), human (*Homo sapiens*, M13295), mouse (*Mus musculus*, U49720), and wallaby (*M. eugenii*, AY286017). The divergence times at all nodes of the evolutionary tree have been obtained from the TimeTree of Life web server (www.timetree.org). The ancestral amino acids at all nodes of the composite phylogenetic tree (fig. S2) have been inferred using PAML (*35*) with JTT and WAG models.

Mutagenesis

AncAmphibian-359 and frog-423 were previously constructed, so their opsin complementary DNAs were inserted into the Eco RI and Sal I restriction sites of the expression vector pMT5 (*22*, *34*). In these pigments, the N and C termini have been replaced by those of the American chameleon (*A. carolinensis*) (Fig. 1) and do not cause any λ_{max} difference among different SWS1 pigments (*22*). To construct chimeric pigments between AncAmphibian-359 and frog423, we replaced all single and multiple segments of Nde I–Hind III (referred to as TM I), Hind III–Bsm BI (TM II), Bsm BI–Sph I (TM III), Sph I–Pst I (TM IV), Pst I–Avr III (TM V), and Avr III–Mfe I (TM VI–VII, or simply TM VI) segments of AncAmphibian S1 by the corresponding regions of frog S1 (fig. S1). Mutant pigments with point mutations were generated by using QuikChange site-directed mutagenesis kits (Stratagene). To rule out spurious mutations, the DNA fragment was sequenced by cycle sequencing reactions using the SequiTherm EXCEL II long-read kits (Epicentre Technologies) with dye-labeled M13 forward and reverse primers. Reactions were run on a LI-COR 4300LD automated DNA sequencer.

The in vitro assay

The clones were expressed in COS1 cells by transient transfection. The pigments were regenerated by incubating the opsins with 11-*cis*-retinal (a gift from R. K. Crouch at Storm Eye Institute, Medical University of South Carolina and the National Eye Institute) and were purified using immobilized 1D4 (The Culture Center) in buffer W1 [50 mM Hepes (pH 6.6), 140 mM NaCl, 3 mM $MgCl_2$, 20% (w/v) glycerol, and 0.1% dodecyl maltoside] (*37*). UV-visible spectra were recorded at 20°C using a Hitachi U-3000 dual-beam spectrophotometer. Visual pigments were bleached for 3 min using a 60-W standard light bulb equipped with a Kodak Wratten #3 filter at a distance of 20 cm. Data were analyzed using SigmaPlot software (Jandel Scientific).

Measuring epistasis

To evaluate all 63 θ values associated with the chimeric pigments, it becomes necessary to infer the λ_{max}s of the nine structurally unstable mutant pigments. Take AncAmphibian-359 with two TM replacements (A34F) as an example. Because A34F is nonfunctional, the TM III and IV of frog-423 together "cannot" shift the λ_{max} of AncAmphibian-359 and $\theta_{3\times4} = 0$ nm. Using $\theta_3 = 51$ nm and $\theta_4 = 1$ nm, $\lambda_{34} = \lambda + \theta_3 + \theta_4 + \theta_{3\times4} = 359 + 51 + 1 + 0 = 411$ nm; similarly, for A134F, $\lambda_{134} = \lambda + \theta_1 + \theta_3 + \theta_4 + \theta_{1\times3} + \theta_{1\times4} + \theta_{3\times4} + \theta_{1\times3\times4} = 359 + 0 + 51 + 1 + 7 + 0 + 0 + 0 = 418$ nm, where λ is the λ_{max} of AncAmphibian-359 (table S2). Hence, either when a new TM change prevents the formation of a structurally stable pigment or when it actually does not shift the λ_{max}, the highest level of the synergistic effect is zero. In this way, we evaluated the λ_{max}s of all 9 unstable and 54 stable pigments, and 63 θ values were determined using 63 simultaneous linear equations (table S2, unstable in bold italics).

The estimation of effects and interactions of amino acid changes (ζs) and TM changes (θs) on the λ_{max}s were conducted using matrix algebra and linear statistical models (*54*). The rows of the coefficient matrix *C* represent the sequences, and the columns represent the effects and interaction to be estimated. The coefficients in the first column of *C* contain all 1s indicating that the ancestral sequence is included in all derived sequences. The elements of the remaining columns have the coefficients (0 or 1) for the individual effects and interactions present in the sequence designated by the row.

The parameters are designated in the column vector X, whereas column vector Y contains the observed λ_{max} values corresponding to the pigments. The simultaneous equations for the observed λ_{max} values are expressed in matrix algebra as:

$$Y = CX,$$

and the estimates of the effects and interactions are obtained by solving the equation for X, that is:

$$X = (C^T C)^{-1}(C^T Y).$$

Because the estimates are linear functions of the observed λ_{max} values, the variance of each estimate is a function of the variances of the λ_{max} values and the coefficient associated with each parameter. For this analysis, the variances for λ_{max} are assumed to be 1 and the covariance 0. Given the variance-covariance matrix for Y is V, the SEs of the estimates are on the diagonal of Se:

$$\mathrm{Se} = \left[(C^T V^{-1} C)^{-1}\right]^{1/2}.$$

Structural analysis

The structures of AncAmphibian S1 and chimeric pigments were obtained by (i) applying homology modeling (Modeller 9v7, www.salilab.org/modeller) to bovine rhodopsin (Protein Data Bank code: 1U19); (ii) adding the missing hydrogen atoms, water molecules, and 11-*cis*-retinal; and (iii) optimizing them first at pure AMBER96 force field level (http://ambermd.org) and then using hybrid quantum mechanical/molecular mechanical (QM/MM) calculations in the ONIOM (our own n-layered integrated molecular orbital and molecular mechanics) electronic embedding scheme (QM = B3LYP/6–31G*; MM = AMBER). It is known that SBN covalently bound to 11-*cis*-retinal is unprotonated

whereas its neighboring E113/D113 is protonated in UV-sensitive pigments. The QM portion of the calculations includes 11-*cis*-retinal with the covalently bound SBN and a hydrogen link atom that saturates the bond cut at the QM and MM boundary.

SUPPLEMENTARY MATERIALS

Supplementary material for this article is available at http://advances.sciencemag.org/cgi/content/full/1/8/e1500162/DC1

Fig. S1. The amino acid sequences of AncAmphibian-359 and frog-423.

Fig. S2. A composite phylogenetic tree of 14 representative SWS1 pigments.

Fig. S3. The tertiary structure of AncAmphibian-359.

Fig. S4. Evolutionary patterns of TM replacements in AncAmphibian-359.

Table S1. Ancestral amino acids with PPs (in parentheses) inferred using PAML with JTT and WAG models.

Table S2. TM changes and associated λ_{max}, $\Delta\lambda_{max}$, θ, and θ_0 ($\Delta\lambda_{max}$ values at the highest levels of epistatic interactions without individual effects) in AncAmphibian-359.

Table S3. The λ_{max} shifts of chimeric mutants caused by various TM replacements that were preceded by other TM replacements.

Table S4. Epistatic evolution of A251643F.

REFERENCES AND NOTES

1. R. A. Fisher, XV.—The correlation between relatives on the supposition of Mendelian inheritance. *Trans. R. Soc. Edinburgh* **52**, 399–433 (1919).
2. S. Wright, Evolution and the Genetics of Populations, Volume 1: Genetic and Biometric Foundations (University of Chicago Press, Chicago, 1968).
3. J. B. Wolf, E. D. Brodie, M. J. Wade, *Epistasis and the Evolutionary Process* (Oxford Univ. Press, Oxford, 2000).
4. M. Lunzer, S. P. Miller, R. Felsheim, A. M. Dean, The biochemical architecture of an ancient adaptive landscape. *Science* **310**, 499–501 (2005).
5. J. Plucain, T. Hindré, M. Le Gac, O. Tenaillon, S. Cruveiller, C. Médigue, N. Leiby, W. R. Harcombe, C. J. Marx, R. E. Lenski, D. Schneider, Epistasis and allele specificity in the emergence of a stable polymorphism in *Escherichia coli*. *Science* **343**, 1366–1369 (2014).
6. D. Dykhuizen, D. L. Hartl, Selective neutrality of 6PGD allozymes in *E. coli* and the effects of genetic background. *Genetics* **96**, 801–817 (1980).
7. D. E. Dykhuizen, A. M. Dean, Evolution of specialists in an experimental microcosm. *Genetics* **167**, 2015–2026 (2004).
8. H. A. Wichman, J. Millstein, J. J. Bull, Adaptive molecular evolution for 13,000 phage generations: A possible arms race. *Genetics* **170**, 19–31 (2005).
9. E. J. Hayden, E. Ferrada, A. Wagner, Cryptic genetic variation promotes rapid evolutionary adaptation in an RNA enzyme. *Nature* **474**, 92–95 (2011).
10. S. Yokoyama, Synthesis of experimental molecular biology and evolutionary biology: An example from the world of vision. *Bioscience* **62**, 939–948 (2012).
11. S. Yokoyama, Synthetic biology of phenotypic adaptation in vertebrates: The next frontier. *Mol. Biol. Evol.* **30**, 1495–1499 (2013).
12. S. Yokoyama, Molecular evolution of vertebrate visual pigments. *Prog. Retin. Eye Res.* **19**, 385–419 (2000).
13. A. Terakita, The opsins. *Genome Biol.* **6**, 213 (2005).
14. S. Yokoyama, F. B. Radlwimmer, The molecular genetics and evolution of red and green color vision in vertebrates. *Genetics* **158**, 1697–1710 (2001).
15. S. Yokoyama, H. Yang, W. T. Starmer, Molecular basis of spectral tuning in the red- and green-sensitive (M/LWS) pigments in vertebrates. *Genetics* **179**, 2037–2043 (2008).
16. S. Yokoyama, J. Xing, Y. Liu, D. Faggionato, A. Altun, W. T. Starmer, Epistatic adaptive evolution of human color vision. *PLOS Genet.* **10**, e1004884 (2014).
17. R. Menzel, W. Backhaus, in *The Perception of Colour*, P. Gousras, Ed. (CRC Press, Boca Raton, FL, 1991), pp. 262–293.
18. L. J. Fleishman, E. R. Loew, M. Leal, Ultraviolet vision in lizards. *Nature* **365**, 397 (1993).
19. J. Viitala, E. Korplmäki, P. Palokangas, M. Koivula, Attraction of kestrels to vole scent marks visible in ultraviolet light. *Nature* **373**, 425–427 (1995).
20. A. T. D. Bennett, I. C. Cuthill, J. C. Partridge, E. J. Maier, Ultraviolet vision and mate choice in zebra finches. *Nature* **380**, 433–435 (1996).
21. S. C. Church, A. T. D. Bennett, I. C. Cuthill, J. C. Partridge, Ultraviolet cues affect the foraging behaviour of blue tits. *Proc. R. Soc. Lond. B* **265**, 1509–1514 (1998).
22. Y. Shi, S. Yokoyama, Molecular analysis of the evolutionary significance of ultraviolet vision in vertebrates. *Proc. Natl. Acad. Sci. U.S.A.* **100**, 8308–8313 (2003).
23. G. H. Jacobs, Ultraviolet vision in vertebrates. *Am. Zool.* **32**, 544–554 (1992).
24. A. T. D. Bennett, I. C. Cuthill, Ultraviolet vision in birds: What is its function? *Vision Res.* **34**, 1471–1478 (1994).
25. D. M. Weinreich, R. A. Watson, L. Chao, Perspective: Sign epistasis and genetic constraint on evolutionary trajectories. *Evolution* **59**, 1165–1174 (2005).
26. D. M. Weinreich, N. F. Delaney, M. A. DePristo, D. L. Hartl, Darwinian evolution can follow only very few mutational paths to fitter proteins. *Science* **312**, 111–114 (2006).
27. M. Lunzer, G. B. Golding, A. M. Dean, Pervasive cryptic epistasis in molecular evolution. *PLOS Genet.* **6**, e1001162 (2010).
28. C. Natarajan, N. Inoguchi, R. E. Weber, A. Fago, H. Moriyama, J. F. Storz, Epistasis among adaptive mutations in deer mouse hemoglobin. *Science* **340**, 1324–1327 (2013).
29. S. Yokoyama, T. Tada, H. Zhang, L. Britt, Elucidation of phenotypic adaptations: Molecular analyses of dim-light vision proteins in vertebrates. *Proc. Natl. Acad. Sci. U.S.A.* **105**, 13480–13485 (2008).
30. F. E. Hauser, I. van Hazel, B. S. W. Chang, Spectral tuning in vertebrate short wavelength-sensitive 1 (SWS1) visual pigments: Can wavelength sensitivity be inferred from sequence data? *J. Exp. Zool. B Mol. Dev. Evol.* **322**, 529–539 (2014).
31. S. Yokoyama, Evolution of dim-light and color vision pigments. *Annu. Rev. Genomics Hum. Genet.* **9**, 259–282 (2008).
32. J. I. Fasick, M. L. Applebury, D. D. Oprian, Spectral tuning in the mammalian short-wavelength sensitive cone pigments. *Biochemistry* **41**, 6860–6865 (2002).
33. Y. Shi, F. B. Radlwimmer, S. Yokoyama, Molecular genetics and the evolution of ultraviolet vision in vertebrates. *Proc. Natl. Acad. Sci. U.S.A.* **98**, 11731–11736 (2001).
34. Y. Takahashi, S. Yokoyama, Genetic basis of spectral tuning in the violet-sensitive visual pigment of African clawed frog, *Xenopus laevis*. *Genetics* **171**, 1153–1160 (2005).
35. Z. Yang, PAML 4: Phylogenetic analysis by maximum likelihood. *Mol. Biol. Evol.* **24**, 1586–1591 (2007).
36. K. R. Babu, A. Dukkipati, R. R. Birge, B. E. Knox, Regulation of phototransduction in short-wavelength cone visual pigments via the retinylidene Schiff base counterion. *Biochemistry* **40**, 13760–13766 (2001).
37. S. Yokoyama, Phylogenetic analysis and experimental approaches to study color vision in vertebrates. *Methods Enzymol.* **315**, 312–325 (2000).
38. A. Altun, K. Morokuma, S. Yokoyama, H-bond network around retinal regulates the evolution of ultraviolet and violet vision. *ACS Chem. Biol.* **6**, 775–780 (2011).
39. S. Yokoyama, R. Yokoyama, Molecular evolution of human visual pigment genes. *Mol. Biol. Evol.* **6**, 186–197 (1989).
40. S. Yokoyama, R. Yokoyama, Adaptive evolution of photoreceptors and visual pigments in vertebrates. *Annu. Rev. Ecol. Syst.* **27**, 543–567 (1996).
41. S. Yokoyama, Molecular genetic basis of adaptive selection: Examples from color vision in vertebrates. *Annu. Rev. Genet.* **31**, 315–336 (1997).
42. T. P. Sakmar, R. R. Franke, H. G. Khorana, Glutamic acid-113 serves as the retinylidene Schiff base counterion in bovine rhodopsin. *Proc. Natl. Acad. Sci. U.S.A.* **86**, 8309–8313 (1989).
43. E. A. Zhukovsky, D. D. Oprian, Effect of carboxylic acid side chains on the absorption maximum of visual pigments. *Science* **246**, 928–930 (1989).
44. J. Nathans, Determinants of visual pigment absorbance: Identification of the retinylidene Schiff's base counterion in bovine rhodopsin. *Biochemistry* **29**, 9746–9752 (1990).
45. T. P. Sakmar, R. R. Franke, H. G. Khorana, The role of the retinylidene Schiff base counterion in rhodopsin in determining wavelength absorbance and Schiff base pK_a. *Proc. Natl. Acad. Sci. U.S.A.* **88**, 3079–3083 (1991).
46. K. Palczewski, G protein–coupled receptor rhodopsin. *Annu. Rev. Biochem.* **75**, 743–767 (2006).
47. T. Tada, A. Altun, S. Yokoyama, Evolutionary replacement of UV vision by violet vision in fish. *Proc. Natl. Acad. Sci. U.S.A.* **106**, 17457–17462 (2009).
48. S. Yokoyama, N. Takenaka, D. W. Agnew, J. Shoshani, Elephants and human color-blind deuteranopes have identical sets of visual pigments. *Genetics* **170**, 335–344 (2005).
49. S. Yokoyama, F. B. Radlwimmer, N. S. Blow, Ultraviolet pigments in birds evolved from violet pigments by a single amino acid change. *Proc. Natl. Acad. Sci. U.S.A.* **97**, 7366–7371 (2000).
50. S. E. Wilkie, P. R. Robinson, T. W. Cronin, S. Poopalasundaram, J. K. Bowmaker, D. M. Hunt, Spectral tuning of avian violet- and ultraviolet-sensitive visual pigments. *Biochemistry* **39**, 7895–7901 (2000).
51. A. M. Dean, J. W. Thornton, Mechanistic approaches to the study of evolution: The functional synthesis. *Nat. Rev. Genet.* **8**, 675–688 (2007).
52. M. J. Harms, J. W. Thornton, Evolutionary biochemistry: Revealing the historical and physical causes of protein properties. *Nat. Rev. Genet.* **14**, 559–571 (2013).
53. G. B. Golding, A. M. Dean, The structural basis of molecular adaptation. *Mol. Biol. Evol.* **15**, 355–369 (1998).
54. F. Graybill, *An Introduction to Linear Statistical Models* (McGraw-Hill, New York, 1961), vol. 1.

55. M. Makino-Tasaka, T. Suzuki, The green rod pigment of the bullfrog, *Rana catesbeiana*. *Vision Res.* **24**, 309–322 (1984).

Acknowledgments: We thank R. Yokoyama, J. Belote, H. Y. Yan, and anonymous reviewers for their comments and R. K. Crouch (Storm Eye Institute, Medical University of South Carolina) and the National Eye Institute for supplying 11-*cis*-retinal. **Funding:** This research was supported by NIH (EY016400 to S.Y.) and Emory University (S.Y.). **Author contributions:** S.Y. designed the study. S.Y. and W.T.S. performed data analyses, and H.J., H.Y., T.K., D.F., and Y.L. constructed chimeric pigments and performed mutagenesis experiments. A.A. performed the QM/MM-based molecular analyses. S.Y., A.A., and W.T.S. wrote the manuscript, with contributions from the other authors. **Competing interests:** The authors declare that they have no competing interests. **Data and materials availability:** The authors confirm that all data underlying the findings and materials are fully available without restriction.

Submitted 12 February 2015
Accepted 2 August 2015
Published 18 September 2015
10.1126/sciadv.1500162

Citation: S. Yokoyama, A. Altun, H. Jia, H. Yang, T. Koyama, D. Faggionato, Y. Liu, W. T. Starmer, Adaptive evolutionary paths from UV reception to sensing violet light by epistatic interactions. *Sci. Adv.* **1**, e1500162 (2015).